

Supporting Information for:

Si/SiO₂-Templated Formation of Ultraflat Metal Surfaces on Glass, Polymer, and Solder Supports: Their Use as Substrates for Self-Assembled Monolayers (SAMs)

Emily A. Weiss[†], George K. Kaufman[†], Jennah K. Kriebel[†], Zhefeng Li[†], Richard Schalek[‡], and George M. Whitesides^{†*}

[†]*Department of Chemistry and Chemical Biology, Harvard University, Cambridge, MA*

[‡]*Center for Nanoscale Systems, Harvard University, Cambridge, MA*

*Corresponding author. FAX: 617-495-2500. Email: gwhitesides@gmwhgroup.harvard.edu

EXPERIMENTAL PROCEDURES

Materials. Ethanol (Aldrich, 200 proof, >99.5% anhydrous) was degassed under argon for ~45 min prior to use, and the 1-hexadecanethiol and heptadecafluoro-1-decanethiol (Aldrich), were passed through neutral alumina to remove polar sulfur compounds. We obtained the (tridecafluoro-1,1,2,3,-tetrahydrooctyl)-1-trichlorosilane from United Chemical Technologies, Inc., the silicon (100) wafers from Silicon Sense (Nashua, NH), the glass slides (7.62 cm × 2.54 cm × 1.2 mm) from VWR, and the optical adhesive (OA, #61) from Norland Products, Inc. We stored the OA in a refrigerator at 4 °C. Sylgard 184 Silicone, a two-part PDMS elastomer, was purchased from Essex Brownell (Edison, NJ). We used a 10:1 (by weight) mixture of PDMS base:curing agent that was degassed under vacuum and cured at 70 °C for 4 h.

Atomic Force Microscopy. AFM micrographs of the metal surfaces were collected in contact-mode or tapping-mode with a Digital Instruments Dimension 3100 Nanoscope, and analyzed using the Nanoscope IV v5.12b18 software package (Digital Instruments, Santa Barbara, CA).

X-Ray Photoelectron Spectroscopy. Spectra were obtained using a Surface Science SSX-100 photoelectron spectrometer using Monochromatic Al K- α X-Ray radiation (1.49 kV, base pressure $\sim 10^{-9}$ Torr). Survey spectra were collected at a constant pass energy of 158 eV from a 1000 μm diameter spot size on the surface. Spectra of the O(1s) core levels were collected at a pass energy of 27 eV with a 600- μm diameter spot size.

Scanning Electron Microscopy. SEM images were acquired with a LEO Scanning Electron Microscope (Zeiss, Model 982) under high vacuum at an electron beam energy of 3 keV and a working distance of 7 mm. The specified resolution of the instrument is 4 nm at 1 keV.

Infrared Spectroscopy. We obtained reflection absorbance infrared (RAIR) spectra (1024 scans at 1 cm^{-1} resolution, baseline-corrected over the range $3100\text{-}2700\text{ cm}^{-1}$) using a Nexus 670 FT-IR spectrometer (Nicolet, Madison, WI) equipped with a surface grazing-angle attachment (SAGA, Thermo Spectra-Tech, Shelton, CT) and an MCT detector that was cooled with liquid nitrogen. The incident reflection angle was set at 80° . The background spectra were taken from a reference silver surface with a SAM of heptadecafluoro-1-decanethiolate on the appropriate mechanical support (e.g., the background spectrum for the Ag film on solder was taken on a SAM of heptadecafluoro-1-decanethiolate on a solder support). The fluorinated SAM minimizes the contributions from the C-H stretching modes of adventitious contaminants.

Scanning Tunneling Microscopy. Images were collected in constant current mode (from 0.5 nA – 1 nA for bare Ag samples to 0.015 nA - 0.05 nA for SAM-covered samples) in a chamber that was equipped with a commercial variable temperature AFM/STM (Omicron Nanotechnology, Taunusstein, Germany). All scans were subject

to background correction. The Pt/Ir tips were purchased from Materials Analytical Sciences (Rayleigh, NC). The scan rate was 3000 nm/s for large area scans (1000 nm × 1000 nm) and ≤ 250 nm/s for the small scans (200 nm × 200 nm). Line profile and roughness analysis was performed using SPIP software, Version 4.3.1.0 (Image Metrology, Denmark).

In general, imaging either the mTS or cTS specimens presented challenges. In both cases molecular scale resolution required high-impedance imaging parameters. Decreasing the gap voltage while keeping the tunneling current constant caused the tip to lose contact with the SAM. Increasing the gap voltage above 2.4 volts was thought to cause electric field desorption of the SAM. Decreasing the tunneling current increased the imaging resolution. (The STM electronics were unable to maintain a constant tunneling current below 1.5 pA. This is an instrument limitation and not a sample-tip limitation.)

Additional Results and Discussion

Analysis of Average Intermolecular Order: Reflection Absorption Infrared Spectroscopy (RAIRs). Figure S4 shows the RAIR spectra of SAMs of SC₁₆ on AS-DEP¹⁻³ and TS silver surfaces (each an average of 1024 scans taken at a resolution of 2 cm⁻¹) after smoothing with 5-point adjacent averaging. Table S1 gives the peak positions, relative amplitudes, and linewidths of the components of these spectra, as determined by fitting them with multi-peak Gaussian functions.

Five bands dominate the IR spectra of SC₁₆ in the bulk crystal and within SAMs on Ag: the symmetric and asymmetric methylene stretching modes, the asymmetric methyl

stretch, and the symmetric methyl stretch. The symmetric methyl stretch is split into two components, (labeled FR₁ and FR₂), due to Fermi resonance interactions with a low-frequency asymmetric methyl deformation mode.^{4,5}

The energies of the symmetric ($\nu_s(\text{CH}_2)$) and asymmetric ($\nu_a(\text{CH}_2)$) methylene stretching modes are especially sensitive to intermolecular packing: the average energies of these vibrations increase with increasing intermolecular disorder. For long-chain alkanethiol molecules in the bulk crystalline phase, their energies are $\nu_s(\text{CH}_2) = 2850\text{-}2851\text{ cm}^{-1}$ and $\nu_a(\text{CH}_2) = 2918\text{ cm}^{-1}$.⁶ The energy of the $\nu_s(\text{CH}_2)$ mode is within the experimental error (2 cm^{-1}) of the bulk crystalline range for all of the samples ($2850\text{-}2852\text{ cm}^{-1}$) except for PDMS/OA, in which case the noise in the spectrum and the breadth of the peaks makes it difficult to derive any structural information from this peak. The position of the $\nu_s(\text{CH}_2)$ band in these spectra suggests that the SAMs on the solder, bare OA, and glass/OA (cTS and mTS) supports, and the SAM on the AS-DEP film, are more like 2D-solids than like 2D-liquids ($\nu_s(\text{CH}_2) = 2855\text{ cm}^{-1}$ for liquid-phase C₈SH).⁶

The energy of the $\nu_a(\text{CH}_2)$ mode is $2917\text{-}2918\text{ cm}^{-1}$ for the SAMs on mTS and cTS silver (on glass/OA), and a 2921 cm^{-1} for the AS-DEP sample. This shift is small, but resolvable, and implies a lower degree of order in the AS-DEP SAM than in the TS SAMs (although the AS-DEP SAM was still more ordered than liquid-phase C₈SH, which has $\nu_a(\text{CH}_2) = 2924\text{ cm}^{-1}$).⁶ The interpretation of the energy of this peak is less straightforward for the SAMs on solder, PDMS/OA, and bare OA. In the spectra for these samples, the $\nu_a(\text{CH}_2)$ peak overlaps with the $\nu_a(\text{CH}_3, \text{FR}_1)$ peak (which appears as a weak shoulder to the $\nu_a(\text{CH}_2)$ peak); the Gaussian fit to this multi-component band is broader and centered at a higher energy than would be the fit to the $\nu_a(\text{CH}_2)$ peak alone.

We suspect that the spectra of the SAMs on bare OA, PDMS/OA, and solder had lower signal-to-noise than did those on glass or Si/SiO₂ substrates because the flexible substrates allowed did not lie completely flat in the spectrometer.⁷

The absence of the bands that correspond to the methyl stretching mode $\nu_s(\text{CH}_3, \text{FR}_2) \sim 2875 \text{ cm}^{-1}$ is another qualitative indicator of structural disorder.⁵ A peak at $\sim 2875 \text{ cm}^{-1}$ is present in all samples, but unresolvable in the spectra of SAMs on PDMS/OA and solder, again, possibly because of a lower signal-to-noise ratio in those samples than in the samples on hard substrates.

The energies of the $\nu_s(\text{CH}_2)$ and $\nu_a(\text{CH}_2)$ peaks for the SAM of SC₁₆ on cTS and mTS silver (glass/OA) are comparable to those reported in the literature for SAMs on evaporated Ag³, Au^{6,8}, and Pt⁹, and suggest that the molecules within these SAMs interact with each other as they would in a bulk crystal of hexadecanethiol. It appears that the SAMs on the solder, bare OA, and PDMS/OA supports are not as well-ordered as the SAM on the glass/OA (mTS and cTS) support, but this statement is difficult to confirm because in general (and especially in the case of the PDMS/OA support), the features in these spectra are broadened, and, in some cases, indistinguishable from the noise.

Post-deposition Annealing. In an attempt to lower the roughness of the TS metal films, we thermally annealed Si/SiO₂/metal (template/film) composites prior to preparing the sandwich structures with the glass/OA support.

Annealing of silver and gold films on Si/SiO₂ in an oven. To minimize the formation of silver oxide, we annealed Ag films on Si/SiO₂ in a vacuum oven, evacuated to a base pressure of 140 mTorr. After the samples were loaded, we increased the temperature of

the oven to 230 °C over the course of 1 h (230 °C is the maximum temperature of the vacuum oven), and held it at 230 °C for an additional hour. The hot Ag films were then used to form sandwich structures with the glass/OA support. We were not concerned about the oxidation of the gold films; the Au films on Si/SiO₂ were, therefore, annealed in a non-vacuum oven. We increased the temperature of the oven to 710 °C (2/3 of the melting point of Au, 1064 °C) over the course of 25 – 30 min, kept the samples at 710 °C for 1 h, and cooled them to room temperature in the oven overnight. We formed sandwich structures with a glass/OA support on the room temperature Au films.

Annealing of silver and gold films on Si/SiO₂ with a flame. As an alternative method for thermally annealing the metal films on Si/SiO₂, we heated the films over a butane flame from a Bunsen burner (temp ~ 1500°C) for 2 min. The metal films faced away from the flame; the Si/SiO₂ wafer directly contacted the tip of the cone of the flame. Only the back (AS-DEP) surface of the films was directly exposed to the atmosphere. We formed sandwich structures with a glass/OA support once the samples had cooled to room temperature in a vacuum desiccator.

The roughness of the gold and silver surfaces increased significantly (Figures S2 and S3) when the metal films were annealed in an oven (Figure S2) or by factors of when the metal films are annealed in a butane flame (Figure S3) before applying the OA/glass backing.

References

- (1) Hines, M. A.; Todd, J. A.; Guyot-Sionnest, P. *Langmuir* 1995, *11*, 493.
- (2) Laibinis, P. E.; Whitesides, G. M.; Allara, D. L.; Tao, Y. T.; Parikh, A. N.; Nuzzo, R. G. *J. Am. Chem. Soc.* 1991, *113*, 7152.

(3) Walczak, M. M.; Chung, C.; Stole, S. M.; Widrig, C. A.; Porter, M. D. *J. Am. Chem. Soc.* 1991, *113*, 2370.

(4) Dubois, L. H.; Nuzzo, R. G. *Annu. Rev. Phys. Chem.* 1992, *43*, 437.

(5) Zhang, M.; Anderson, M. R. *Langmuir* 1994, *10*, 2807.

(6) Porter, M. D.; Bright, T. B.; Allara, D. L.; Chidsey, C. E. D. *J. Am. Chem. Soc.* 1987, *109*, 3559.

(7) The background spectra for all samples were taken on the same substrates as the spectra of the SAMs of hexadecanethiolate, so the spectrum of PDMS, which has features in this region of the IR, has already been subtracted from the spectrum shown in Figure 8.

(8) Stole, S. M.; Porter, M. D. *Langmuir* 1990, *6*, 1199.

(9) Petrovykh, D. Y.; Kimura-Suda, H.; Opdahl, A.; Richter, L. J.; Tarlov, M. J.; Whitman, L. J. *Langmuir* 2006, *22*, 2578.

Supporting Figure Captions.

Figure S1. Contact-mode AFM micrographs of the TS Au (**a**) and TS Ag (**b**) surfaces (on glass/OA support) mechanically cleaved (in air) after dipping the entire sandwich structure in liquid N₂ for 30 s. The vertical scales on the oblique-view images are 75 nm/division for (**a**) and 12.5 nm/division for (**b**). The RMS roughnesses of the surfaces (total area = 25 μm²) are 0.7 nm (Au) and 6.1 nm (Ag).

Figure S2. a) Contact-mode AFM micrograph of the TS Au surface formed when the gold was annealed at 710°C for 1 h before application of the glass/OA support. The RMS roughness of the surface (total area = 25 μm²) is 10.3 nm. **b)** Contact-mode AFM micrograph of the Ag surface formed when the Ag was annealed at 230 °C for 1 h before

application of the glass/OA support. The vertical scales on the oblique-view images are 20 nm/division for (a) and 17.5 nm/division for (b). The RMS roughness of the surface (total area = 25 μm^2) is 6.9 nm.

Figure S3. Contact-mode AFM micrographs of Au (a) and Ag (b) surfaces formed when the films were annealed in a butane flame for 2 min before application of the glass/OA support. The vertical scales on the oblique-view images are 12.5 nm/division for (a) and 40 nm/division for (b). The RMS roughnesses of the surfaces (total area = 25 μm^2) are 1.4 nm (Au) and 6.2 nm (Ag).

Figure S4. Plots of the C-H stretching region of the RAIR spectra (after 5-point smoothing) for the SAM Ag-SC₁₆ on TS silver (with PDMS/OA, solder, bare OA, and glass/OA mechanical supports), and on AS-DEP silver. The y-axes of these spectra were rescaled for purposes of presentation (hence, there are no labels on this axis). The mTS samples were mechanically template-stripped in air and then immediately put into an ethanolic solution of hexadecanethiol, and cTS samples were chemically template-stripped under the solution of hexadecane thiol (as described in the text). The peak positions and amplitudes of the components of multi-peak Gaussian fits to the smoothed spectra are given in Table S1. Dashed vertical lines at 2851 cm^{-1} (symmetric CH₂ stretch) and 2918 cm^{-1} (asymmetric CH₂ stretch) indicate the energies of long-chain alkanethiol molecules in the bulk crystalline phase.

Figure S5. Absolute value of current vs. voltage ($|I|$ - V) curves acquired by the STM tip on **a)** three separate locations on a bare Ag (mTS) surface, **b)** six separate locations on a SAM of SC₁₂ on cTS Ag (three within ordered regions of the SAM and three within disordered regions of the SAM), **c)** six separate locations on a SAM of SC₁₂ on mTS Ag (one within an ordered region of the SAM and five within disordered regions of the SAM). The ordered SAMs formed on flat {111} planes of the Ag surface; the disordered SAMs formed on highly-tilted terraces and non-{111} planes of the Ag surface. These plots demonstrate that there were molecules present in the tunneling gap, even in the disordered regions of the SAM: The current recorded on the bare Ag surface is consistently at least a factor of ten higher, and more symmetric around $V = 0$, than those recorded on the SAMs. The asymmetry of the I - V curves for the SAMs (and the fact that their minima do not lie at $V = 0$) is probably due to a combination of i) the asymmetry of the junction resulting from the gap between the SAM and the tip (necessary for high-impedance measurements), and ii) accumulation of charge at one of the contacts due to the low conductivity of the monolayer.

Figure S6. a) XP spectrum of a drop of UV-cured OA, and (b) N 1s and (c) S 2p peaks from the XP spectra of OA, TS (glass/OA), and AS-DEP silver surfaces. The spectra in (b) and (c), from top to bottom, correspond to AS-DEP silver with a SAM of SC₁₆, mTS silver with a SAM of SC₁₆, cTS silver with a SAM of SC₁₆, bare AS-DEP silver, bare mTS (glass/OA) silver, bare mTS (glass/OA) silver placed in neat ethanol for 12 h, and OA. OA is composed of approximately 64.5% C, 22.5% O, 6.5 % S, and 6.4 % N. All peaks in the spectrum for OA (including the N 1s peak shown in (b) and S 2p peak shown

in (c)) are shifted to higher energy by 4–4.5 eV due to charging of the non-conductive OA in the spectrometer. There is no perceptible nitrogen in any of the silver samples. The baselines of the spectra in (b) are slanted because this region overlaps with that of the Ag 3d energy loss (inelastic scattering) peak. Sulfur is present in the silver samples that contain a SAM; there is no perceptible sulfur in the silver samples that contain no SAM.

Figure S7. SEM image of a representative portion of the interior of the TS Ag film on a PDMS/OA support after bending it at $\theta_{\text{rad}} = 100^\circ$. The images were taken at an electron beam energy of 3 keV and a working distance of 7 mm. **b)** Tapping-mode AFM micrographs of the Ag surface before and after bending it at $\theta_{\text{rad}} = 160^\circ$. The RMS roughness of the surface (over a $25 \mu\text{m}^2$ area) was 0.8 nm before bending and 1.1 nm after bending.

Table S1. Energies of the Vibrational Modes of SAMs of SC₁₆ on TS Ag from Multi-Gaussian Fits of RAIR Spectra

Mechanical Support (Preparation)	Lineshape Parameters for Each Major Vibrational Mode ^{a,b}									
	ν _s (CH ₂)		ν _a (CH ₂)		ν _a (CH ₃)		ν _s (CH ₃ , FR ₁)		ν _s (CH ₃ , FR ₂)	
	Energy (Amp.)	FWHM	Energy (Amp.)	FWHM	Energy (Amp.)	FWHM	Energy (Amp.)	FWHM	Energy (Amp.)	FWHM
Solder (mTS)	2851 (0.23)	7.8	2923 (1)	20.7	2963 (0.48)	10.7	--		--	
PDMS/OA (mTS)	2859 (1.35)	53.8	2921 (1)	34.4	2959 (0.27)	20.3	--		--	
bare OA (mTS)	2852 (0.13)	11.3	2924 (1)	28.3	2962 (0.92)	22.7	--		2878 (0.99)	38.2
glass/OA (mTS)	2850 (0.57)	9.2	2918 (1)	21.0	2964 (1.66)	10.9	2937 (0.62)		2878 (1.08)	21.2
glass/OA (cTS)	2851 (0.71)	12.5	2917 (1)	14.0	2965 (0.89)	11.7	2932 (1.2)	11.7	2878 (0.43)	18.2
n/a (AS-DEP)	2851 (0.35)	8.7	2921 (1)	14.0	2964 (0.37)	8.9	2936 (0.23)	10.5	2877 (0.08)	5.9

^aThe parameters are: energy (in cm⁻¹), amplitude of the component (Amp., in parentheses, normalized to the amplitude of the ν_a(CH₂) component), and full-width-at-half-max of the band, FWHM, in cm⁻¹. ^bThe symbol "--" indicates that no component with a maximum near this frequency contributed to the total fit.

Figure S1.

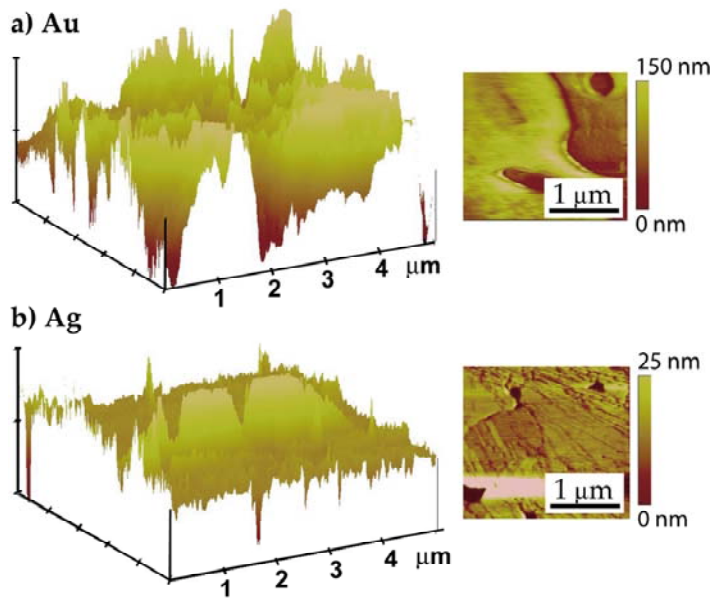


Figure S2.

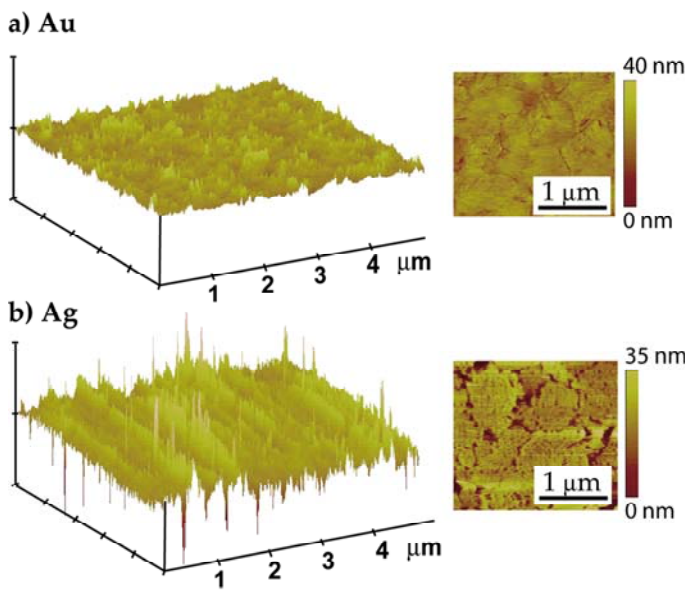


Figure S3.

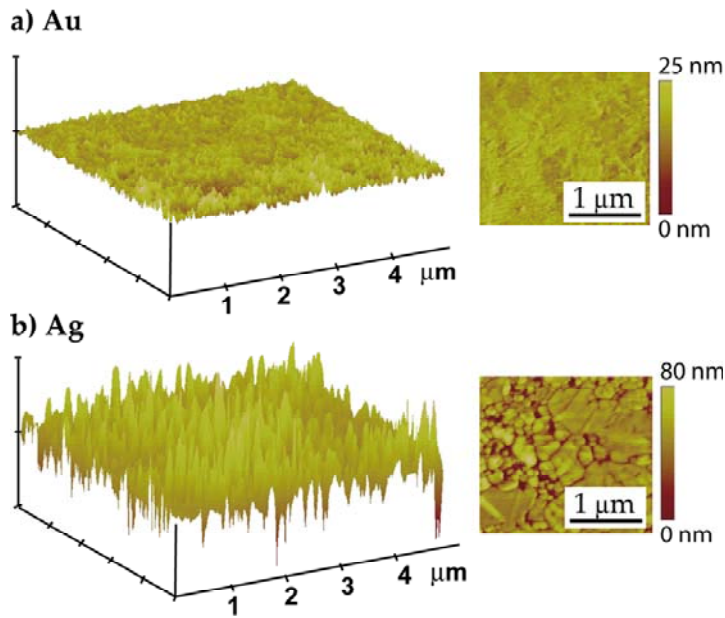


Figure S4.

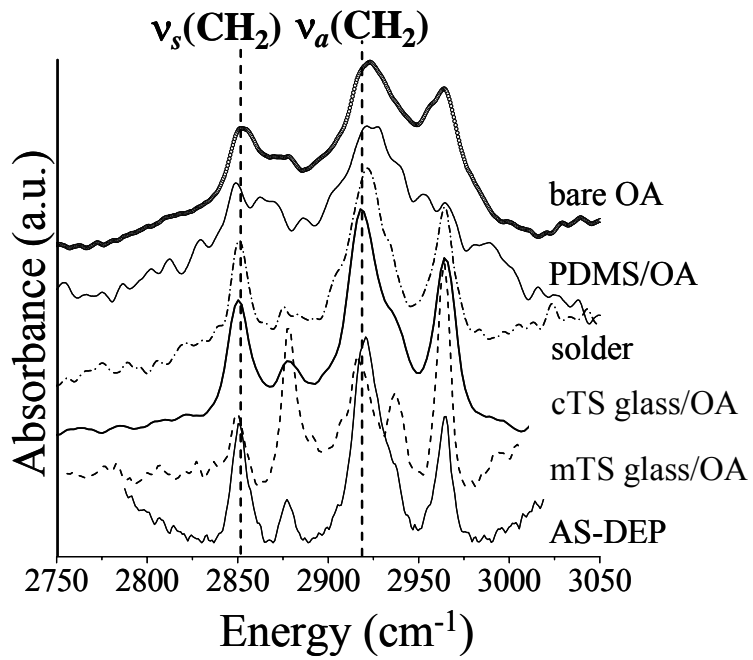


Figure S5.

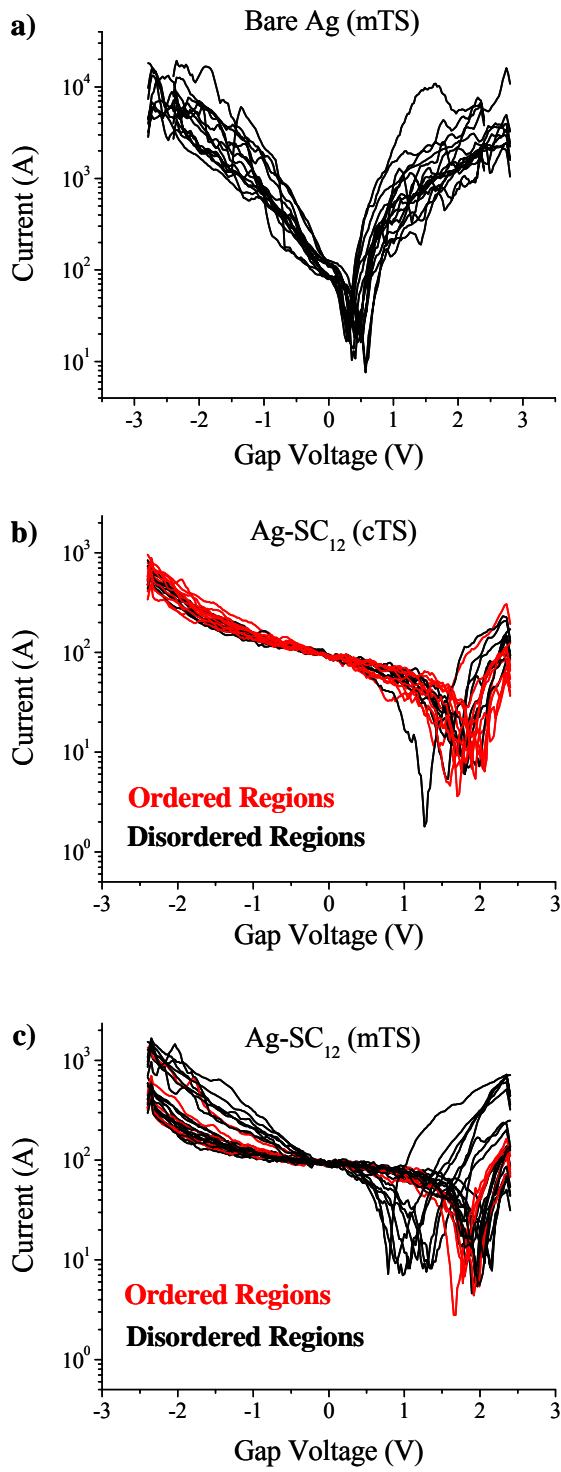


Figure S6.

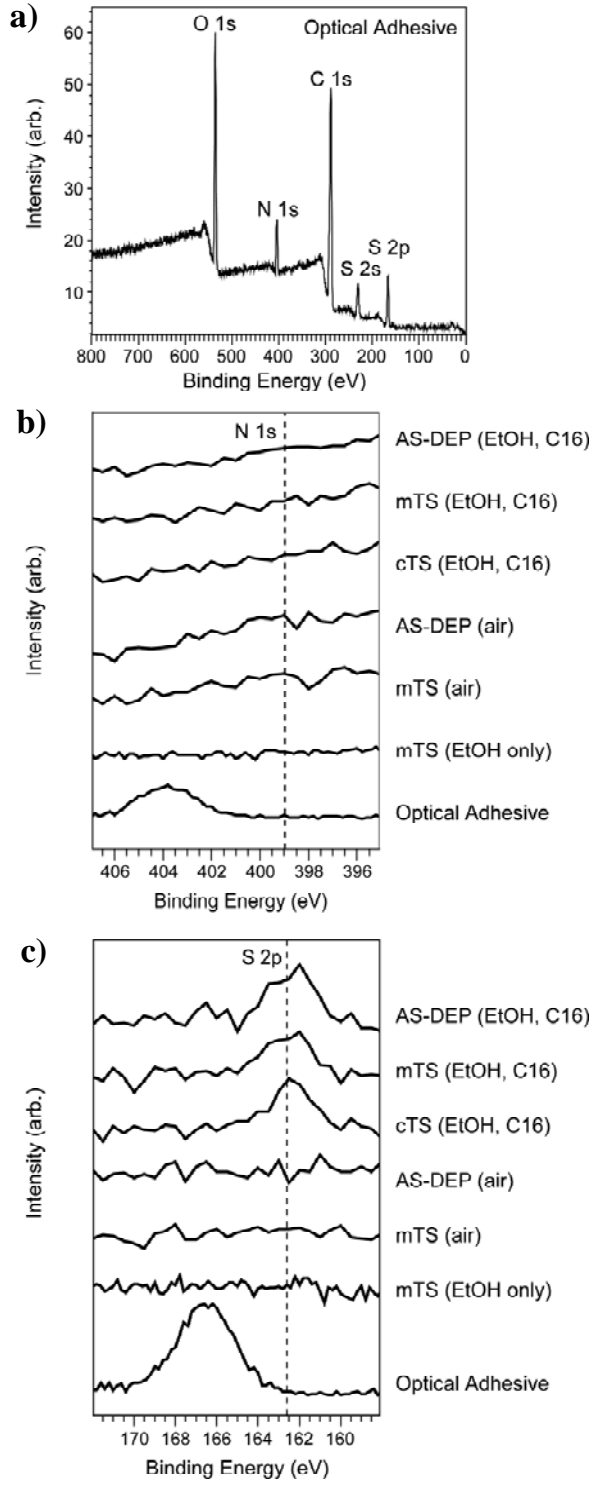


Figure S7.

